Subcellular niche segregation of co-obligate symbionts in whiteflies

Akiko Fujiwara[a,b], Xian-Ying Meng[c], Yoichi Kamagata[c], and Tsutomu Tsuchida[d#]

[a] Center for Food Science and Wellness, Gunma University, Maebashi 371-8510, Japan

[b] Chemical Genomics Research Group, RIKEN Center for Sustainable Resource Science, Wako, 351-0198, Japan

[c] Bioproduction Research Institute, National Institute of Advanced Industrial Science and Technology, Tsukuba 305-8566, Japan

[d] Faculty of Science, Academic Assembly, University of Toyama, 3190 Gofuku, Toyama City, Toyama, 930-8555, Japan

Running title

Subcellular niche segregation of the symbionts

#Corresponding author:

Tsutomu Tsuchida

tsuchida@sci.u-toyama.ac.jp

+81-76-445-6553

ORCID:

Akiko Fujiwara: 0000-0001-7814-5611

Yoichi Kamagata: 0000-0001-7124-5812

Tsutomu Tsuchida: 0000-0001-6065-4469

Abstract

Many insects contain endosymbiotic bacteria within their bodies. In multiple endosymbiotic systems comprising two or more symbionts, each of the symbionts is generally localized in a different host cell or tissue. *Bemisia tabaci* （Sweet potato whitefly）possesses a unique endosymbiotic system where co-obligate symbionts are localized in the same bacteriocytes. Using fluorescence *in situ* hybridization, we found that endosymbionts in *B. tabaci* MEAM1 occupy distinct subcellular habitats, or niches, within a single bacteriocyte. *Hamiltonella* was located adjacent to the nucleus of the bacteriocyte, while *Portiera* was present in the cytoplasm surrounding *Hamiltonella*. Immunohistochemical analysis revealed that the endoplasmic reticulum separates the two symbionts. Habitat segregation was maintained for longer durations in female bacteriocytes. The same segregation was observed in three genetically distinct *B. tabaci* groups (MEAM1, MED Q1, and Asia II 6) and *Trialeurodes vaporariorum*, which shared a common ancestor with *Bemisia* over 80 million years ago, even though the coexisting symbionts and the size of bacteriocytes were different. These results suggest that the habitat segregation system existed in the common ancestor and was conserved in both lineages, despite different bacterial partners coexisting with *Portiera*. Our findings provide insights into the evolution and maintenance of complex endosymbiotic systems

and highlight the importance of organelles for the construction of separate niches for endosymbionts.

Importance

Co-obligate endosymbionts in *B. tabaci* are exceptionally localized within the same bacteriocyte (a specialized cell for endosymbiosis), but the underlying mechanism for their coexistence remains largely unknown. This study provides evidence for niche segregation at the subcellular level between the two symbionts. We showed that the endoplasmic reticulum is a physical barrier separating the two species. Despite differences in co-obligate partners, this subcellular niche segregation was conserved across various whitefly species. The physical proximity of symbionts may enable the efficient biosynthesis of essential nutrients via shared metabolic pathways. The expression "Good fences make good neighbors" appears to be true for insect endosymbiotic systems.

Author contributions: A.F. and T.T. designed research; A.F. and Y.M. performed research; Y.K. contributed new analytic tools; A.F. and T.T. analyzed data and wrote the paper.

Introduction

Numerous insects contain endosymbiotic bacteria within their bodies. Some endosymbionts are obligate, with crucial roles in host growth and reproduction, by providing essential nutrients, while others are facultative (1, 2). In multiple endosymbiotic systems comprising two or more symbionts, each of the symbionts is generally localized in a different host cell or tissue. This type of localization is observed in various insect species, such as aphids, spittlebugs, leafhoppers, scale insects, adelgids, psyllids, and cicadas (1, 3-13) (*Supporting data only for review* in Supplemental Information). The compartmentalization of multiple symbionts into different host cells is considered as an important step in evolution, to reduce direct conflict between the multiple symbionts and control them within the same host (12, 14).

The sweet potato whitefly *Bemisia tabaci* (Hemiptera: Aleyrodidae) is a cryptic species complex comprising more than 44 genetic groups based on the mitochondria cytochrome oxidase I sequences (15). Among the genetic groups, Middle East Asia Minor 1 (MEAM1) and Mediterranean Q1 (MED Q1) are globally important pests, and both possess two phylogenetically distinct types of endosymbiotic bacterium, *Candidatus* Portiera aleyrodidarum and *Candidatus* Hamiltonella defense (hereinafter called *Portiera* and *Hamiltonella*, respectively). They are co-obligate symbionts based on the virtually universal infection observed in natural populations (16-23), the decrease in host fitness caused by symbiont elimination (24, 25), and their genome contents for producing essential amino acids and cofactors (26-29), although mathematical metabolic models assuming limited conditions suggested that *Hamiltonella* shows a nutritionally parasitic state (30).

Interestingly, previous studies have reported that these symbionts in *B. tabaci*

are co-localized in the same bacteriocytes (31-33), suggesting possible competition between the symbionts for limited space and resources. Nevertheless, *Portiera* and *Hamiltonella* populations are large and exhibit synchronous dynamics in MEAM1 (34). These data suggest that some mechanism exist to maintain the two essential symbionts in the same bacteriocytes. One mechanism for avoiding conflict between the symbionts would be niche segregation, although it has never been reported at the subcellular level. In this study, we demonstrated that habitats of the symbionts are segregated within a single bacteriocyte by the endoplasmic reticulum (ER). Our results also suggest that this segregation system operates not only in specific genetic groups of *B. tabaci* but also in other whitefly species.

Results and Discussion

Temporal dynamics of co-obligate symbionts

We used quantitative polymerase chain reaction (PCR) to investigate the population dynamics of the two symbiotic bacteria *Portiera* and *Hamiltonella* in MEAM1. Both populations increased during nymphal growth, peaked in actively reproducing young adults, and declined in older whiteflies (Fig. S1). The primary role of these symbionts is to provide nutrients to the host (26-29). Consistent with that role, their population dynamics correspond to the necessity for the host growth and reproduction, as reported for other obligate symbionts of multiple insect hosts, including the pea aphid (35-37), cereal weevils (38), and a different MEAM1 strain (34). The populations of both symbionts in females were maintained at relatively higher levels for longer durations than those for the male populations (Fig. S1). These results suggest that the symbiont

113 populations are differentially regulated depending on the host's sex.

114

115 **_Portiera_ and _Hamiltonella_ occupy the same bacteriocytes but segregate into different**
116 **subcellular niches**

117 Previous studies using FISH analysis (39, 40) suggested that
118 *Hamiltonella* is distributed around the nucleus of the bacteriocyte while
119 *Portiera* is distributed in the cytoplasmic regions. However, the distribution
120 pattern was not clear as the observations were made on a single slice of the bacteriocyte.
121 Therefore, we acquired 3D spatial data depicting the distribution of the two symbionts in
122 bacteriocytes using Z stack analysis. Confocal laser scanning microscopy of the teneral
123 adults of MEAM1 revealed distinct niche for the two symbionts within the same
124 bacteriocytes: *Hamiltonella* was located adjacent to the nucleus of the bacteriocyte, while
125 *Portiera* was located in the cytoplasm, surrounding *Hamiltonella* (Fig. 1A, Movie S1). In
126 contrast, *Rickettsia,* which generally infects MEAM1 as a facultative symbiont (16, 19-
127 23, 41, 42), were scattered all over the body and rarely observed in the bacteriocytes (Fig.
128 S2*A* and *B*).

129 In *B. tabaci*, an intact bacteriocyte-bearing symbiont is transferred to each egg in
130 adult females (43) that persists through embryogenesis (44). Niche segregation between
131 *Portiera* and *Hamiltonella* was observed in the bacteriocytes transferred into the eggs (Fig.
132 1*B*) of MEAM1 and was maintained from nymphs (Fig. 1*C*) to female and male young
133 adults (Fig. S3*A* and *B*), during which the metabolic function of the symbionts becomes
134 necessary for host growth and reproduction. At 15 d after adult eclosion, the observed
135 habitat segregation was disrupted only in male bacteriocytes (Fig. S3*C* and *D*). This

136 observation was consistent with the report that apoptosis and autophagy occurred in male
137 bacteriocytes but not in females (33). *Portiera* and *Hamiltonella* titers remarkably
138 declined only in males at this stage (Fig. S1); hence it is conceivable that the long-term
139 stable habitat in female bacteriocytes evolved to ensure the vertical transmission of both
140 symbionts.
141
142 **The endoplasmic reticulum segregates symbionts within bacteriocytes**
143 We performed electron microscopy to further understand the mechanisms
144 underlying the subcellular niche segregation of symbionts in bacteriocytes. The results
145 revealed the presence of rod-shaped bacteria next to the nucleus and unstructured
146 hypertrophic bacteria on the outer cytoplasm (Fig. 2*A*). The shapes and locations of the
147 two bacteria types were consistent with those of *Hamiltonella* and *Portiera,* as
148 demonstrated by FISH (Fig. 1*A*–*C*). Interestingly, an ER-like multiple membrane structure
149 was observed around *Hamiltonella* (Fig. 2*B*).
150 The ER and *Hamiltonella* were simultaneously detected using a combination of
151 immunohistochemistry and FISH at the young adult stage. Strong fluorescence signals for
152 the ER marker were detected around the nuclei of bacteriocytes and surrounded the
153 fluorescence signals for *Hamiltonella* (Fig. 3*A* and Fig. S4*A*). A three-dimensional
154 analysis using composite Z-stack images revealed that the ER encompassed *Hamiltonella*
155 (Fig. 3*A*). These results confirmed that the ER partitioned *Hamiltonella* and *Portiera*. At
156 15 d after adult eclosion, the ER and cell structure disruption was observed in males (Fig.
157 S4*C*), possibly due to programmed cell death (33). In comparison, the ER was detected
158 between the co-obligate symbionts in females (Fig. S4*B*). These results indicate that the

ER-mediated subcellular niche segregation of the symbionts lasts longer in females. It suggests that the ER has an important role in maintenance of stable niche for each symbiont especially in female bacteriocytes which are needed to be transferred to the next generation (44).

Subcellular niche segregation in other *B. tabaci* subgroups and more distantly related species

The *B. tabaci* subgroup MED Q1 also possesses *Portiera* and *Hamiltonella* as co-obligate symbionts (16-21, 26). FISH analysis indicated that *Portiera* and *Hamiltonella* are segregated within individual bacteriocytes through earlier developmental stages in MED Q1 (Fig. 1*D–F*), as observed in MEAM1 (Fig. 1*A–C*). The facultative symbiont *Cardinium* in MED Q1 did not show specific localization in bacteriocytes (Fig. S2*C* and *D*). Combining FISH and immunohistochemistry, the ER membrane encompassed *Hamiltonella* and separated it from *Portiera* (Fig. 3*B* and Fig. S4*D*). Cytological staining of the dissected living bacteriocytes from young adults also demonstrated that *Hamiltonella* was sterically surrounded by the ER and was segregated from *Portiera* (Fig. S5).

Furthermore, we assayed for subcellular habitat segregation in a distantly related genetic group of *B. tabaci*, Asia II 6. Asia II group is frequently infected with *Candidatus* Arsenophonus sp. (hereafter called *Arsenophonus*) in addition to *Portiera* but not with *Hamiltonella* (19, 20, 45). Using FISH, we demonstrated that *Arsenophonus* is located adjacent to the nucleus of the bacteriocyte in both adults and developing eggs (Fig. 4). The localization pattern of *Arsenophonus* in Asia II 6 was identical to that of

182 *Hamiltonella* in both MEAM1 (Fig. 1*A*–*C*) and MED Q1 (Fig. 1*D*–*F*). Moreover,
183 *Arsenophonus* around the nucleus was surrounded by the ER (Fig. S4*E*), similar to that of
184 *Hamiltonella* in MEAM1 and MED Q1 (Fig. S4*A*, *B* and *D*).

185 *Trialeurodes vaporariorum* belongs to the same family as *B. tabaci*,
186 *Aleyrodinae* (46). *Arsenophonus* has been detected at high frequencies in *T. vaporariorum*
187 (22, 32, 47, 48) and is considered an essential symbiont, supplying or complementing the
188 nutrients that are not produced by coexisting *Portiera* (49). FISH revealed that *Portiera*
189 and *Arsenophonus* also exhibit subcellular habitat segregation in the same bacteriocytes
190 of *T. vaporariorum* (Fig. 5*A*). Immunohistochemical staining with FISH indicated that the
191 ER encloses *Arsenophonus,* separating it from *Portiera* (Fig. 5*B* and Fig. S4*F*).
192 Bacteriocytes in *T. vaporariorum* (ca. 20 μm in diameter) are considerably smaller than
193 those of *B. tabaci* (ca. 30 to 50 μm). Despite the morphological and phylogenetic
194 differences, the same system in bacteriocytes is involved in symbiont niche partitioning.
195 This suggests that the subcellular niche segregation of the symbionts evolved in the
196 common ancestor and have been conserved to the present.
197

198 **Biological implications, evolution, and possible mechanisms underlying subcellular**
199 **symbiont segregation**

200 Previous ecological studies have shown that niche segregation reduces the
201 strength of competition between species that exploit the same limiting resource (50-52).
202 Niche segregation is found in various taxa, including endosymbiotic bacteria in insects, in
203 which each endosymbiont generally localizes in different host cells or organs (1, 3-12).
204 The compartmentalization of multiple symbionts into different host cells is considered as

an important step in the evolution to reduce direct conflict between the multiple symbionts and control them within the same host (14). The endosymbiotic system in *B. tabaci* is a rare exception because co-obligate symbionts occupy the same bacteriocytes (31, 32). In this study, we revealed that the endosymbionts in *B. tabaci* and *T. vaporariorum* are separated by the ER and show niche segregation at the subcellular level. This novel finding indicates that the niche segregation of endosymbionts can be established not only in different host cells but also within a single cell.

It is intriguing why the symbiont co-habitation has evolved exceptionally in the whiteflies. In certain whitefly species, including *B. tabaci* and *T. vaporariorum*, one or more entire bacteriocytes bearing symbionts are transferred to the developing egg (1, 43, 44, 53). Under the unique transmission manner, one of the symbiont partners could be lost by the failure of transmission if the two co-obligate symbiotic bacteria were separated into different cells. Hence, it is conceivable that the unique transmission machinery of the symbionts has driven the evolution of the symbiont co-localization in whiteflies. To clarify the evolutionary process of co-habitation and subcellular niche segregation of the symbionts, further studies are required on the vertical transmission and localization manners of the symbionts in various whitefly species.

In some co-obligate symbiotic systems in insects, each symbiont can complete the biosynthetic pathway of some essential nutrients, such as essential amino acids or vitamins, on its own or with host genes (13, 54-58). In other co-symbiotic systems, metabolic interdependence for some essential nutrients is present, wherein one of the symbionts possesses genes necessary for the first part of the biosynthetic pathway, and the other symbiont has genes necessary for the latter part of the pathway (10, 12, 13, 59-60). In such a system, metabolic intermediates must diffuse or be translocated from one

symbiont to another to produce essential nutrients in adjacent host cells. However, the co-obligate symbiotic system in *B. tabaci* has a more complex interdependence; enzymes for essential amino acids (*e.g.,* lysine) are dispersed across both *Portiera* and *Hamiltonella*, and metabolic intermediates should be transported between the symbionts multiple times for production (26-28) (Fig. S6*A*). Although several metabolic duplications are present in the host genome (27, 28, 61), the physical proximity between *Portiera* and *Hamiltonella* in the same bacteriocyte, which is stably maintained during development (Fig. 1), may be adaptive for the efficient production of essential amino acids using intertwined biosynthetic pathways (Fig. S6*C*). It should be noted that mealybugs also have intertwined metabolic pathways in their co-obligate symbiotic systems; gamma-proteobacteria are located inside the beta-proteobacterium *Tremblaya*, and metabolic intermediates are transported between them multiple times to produce nutrients (62-65). Accordingly, reducing the distance between symbionts could be a driving force for the evolution of complex interdependent biosynthetic pathways.

B. tabaci is a cryptic species complex with reportedly more than 44 genetic groups (15). In this study, we found the subcellular habitat segregation of two symbionts in three distinct genetic groups in *B. tabaci*, MEAM1, MED Q1, and Asia II 6 (Fig. 1, 4 and Fig. S4*A*-*E*). Moreover, the same localization pattern of symbionts was detected in *T. vaporariorum* (Fig. 5 and Fig. S4*F*) belonging to the different genera. In Asia II 6 and *T. vaporariorum*, the subcellular niche occupied by *Hamiltonella* in MEAM1 and MED Q1 was occupied by *Arsenophonus*. Similar to *Hamiltonella* in *B. tabaci*, it has been suggested that *Arsenophonus* shares metabolic pathways for essential amino-acid synthesis with *Portiera* and the host *T. vaporariorum* (Fig. S6*B*) (49, 66). *Arsenophonus* might establish co-obligate symbiotic systems with *Portiera* in Asia II 6 as well as in *T.*

253 *vaporariorum*. In many geographic regions, *Hamiltonella* and *Arsenophonus* are rarely
254 found in the same individual of *B. tabaci* and *T. vaporariorum* (16-23, 67), suggesting
255 that the two symbiotic bacteria are competing over functional and cytological niches.
256 Moreover, it appears that the habitat segregation system was established in a common
257 ancestor of species in *Aleyrodinae* and was conserved, while the bacterial partners
258 coexisting with *Portiera* have been replaced (Fig. 6). To understand the generality and the
259 evolutionary origin of the habitat segregation system, detailed analyses of other genetic
260 groups in *B. tabaci* and diverse whitefly species are required.

261 As mentioned above, the bacterial partner coexisting with *Portiera* in
262 bacteriocytes varied depending on the species and groups of host insects. This indicates
263 that some molecular and cellular mechanisms underlying subcellular habitat segregation
264 are mainly attributed to the host insects. It is also possible that the symbionts in whiteflies
265 have some properties associated with the ER in bacteriocytes. It is noteworthy that human
266 pathogenic bacteria, such as *Legionella pneumophila, Brucella abortus,* and *Simkania*
267 *negevensis,* exploit the host ER to generate a niche for replication (68-71). Recent studies
268 have revealed that the organelles have an intimate association with endosymbiotic bacteria
269 and play key roles in the maintenance and control of the endosymbiotic system in insects
270 (72-76). This study provides novel insight into the interaction between symbionts and
271 organelles. To clarify the molecular mechanisms underlying subcellular niche segregation,
272 further studies are required from the perspectives of both the host and the symbionts.
273 Super-resolution microscopy and cryo-electron microscopy will be useful in revealing
274 details about the sites of interaction between the symbionts and ER and inferring
275 molecular mechanisms.
276

Materials and methods

Materials. Whitefly strains and their symbionts used in the study are listed in Table S1. *Bemisia tabaci* was maintained on cabbage (*Brassica oleracea*) and *Trialeurodes vaporariorum* on cucumber (*Cucumis sativus*) at 25 ± 1°C and 40–60% relative humidity in a long-day regimen (16L: 8D). Adult *B. tabaci* Asia II 6 insects were collected from the field in May 2017 and immediately stored in 100% acetone until use (77). Additional detailed information is provided in Table S1 and Fig. S7.

DNA extraction and quantitative PCR analysis of symbionts. Ten individuals of MEAM1 at each developmental stage (Fig. S7), from egg to adult, were collected. Eggs and nymphs were collected without distinction between males and females as the sex of whiteflies is indistinguishable at immature stages. In the adult stages, whiteflies from both sexes were separately collected. Samples were preserved in 100% acetone (77) until DNA extraction. The total genomic DNA of the insect individual and its symbionts was extracted using the NucleoSpin Tissue XS Kit (MACHEREY-NAGEL, Duren, Germany), according to the manufacturer's instructions. From the eggs, the DNA was extracted from groups of 10 individuals. *Portiera* and *Hamiltonella* were quantified in terms of 16S ribosomal RNA gene copies using the Mx3005P system (Agilent Technologies, Santa Clara, CA, USA) with THUNDERBIRD SYBR qPCR Mix (Toyobo, Osaka, Japan), and specific primer sets (Table S2). PCR conditions were: 95°C for 3 min, followed by 40 cycles of 95°C for 30 s and 55°C for 30 s, and a final extension at 72°C for 30 s. The

quantitative PCR analysis was conducted by using a standard curve method, as described previously (78).

Fluorescence *in situ* hybridization (FISH). To examine the localization of the symbionts, the insect whole-body or dissected tissue specimens were fixed in Carnoy's solution (EtOH: chloroform: glacial acetic acid, 6:3:1), bleached in 6% hydrogen peroxide in EtOH, and subjected to whole-mount FISH, as described (79). Fluorochrome-labelled oligonucleotide probes are listed in Table S2. Host-cell nuclei were counterstained with 4,6-diamino-2-phenylindole (DAPI). The specificity of *in situ* hybridization was confirmed using a no-probe control and an RNase digestion control (78).

Transmission electron microscopy. Twenty teneral adults of MEAM1 (1 d old after eclosion) were dissected in 2.5% glutaraldehyde in 0.1 M phosphate buffer (pH 7.4), and the dissected bacteriocytes were pre-fixed with the fixative at 4°C overnight. Subsequently, the samples were post-fixed with 2% osmium tetroxide in 0.1 M phosphate buffer (pH 7.4) at 4°C for 90 min before dehydration with a graded ethanol series. The dehydrated specimens were embedded in EPON 812 resin, processed into ultrathin sections (approximately 80 nm thick) using an ultramicrotome EM UC7 (Leica, Wetzlar, Germany), mounted on copper meshes, stained with uranyl acetate and lead citrate, and observed under a transmission electron microscope (80kV; H-7600 Hitachi, Tokyo, Japan).

Simultaneous detection of symbionts and endoplasmic reticulum. Ten to twenty

323 mixed-sex individuals of 1–5 d or 15 d after adult eclosion were collected from the
324 laboratory strains, *B. tabaci* MEAM1 and MED Q1 and *T. vaporariorum* (Table S1). For
325 *B. tabaci* Asia II 6, acetone-preserved samples were used owing to the difficulty of
326 obtaining fresh materials. After samples were washed with 70% EtOH, bacteriocytes were
327 collected by dissection in phosphate-buffered saline (PBS). The bacteriocytes were
328 transferred to 6.5-mm Transwell dishes with 8-μm pore polycarbonate membrane inserts
329 (Corning, New York, NY, USA) and fixed in 4% paraformaldehyde (PFA in phosphate
330 buffer) for 3 h at 25°C. After fixation, bacteriocytes were washed thrice in PBS with 0.3%
331 TritonX-100 (PBSTx) for 30 min and then soaked thrice in hybridization solution (20 mM
332 Tris-HCl pH 8.0, 0.9 M NaCl, 0.01% SDS and 30% formamide) for 5 min. Then,
333 fluorochrome-labeled probes were hybridized overnight at 25°C. The oligonucleotide
334 probes (Table S2) were used for *Portiera* detection. For *Hamiltonella* or *Arsenophonus*
335 detection, Stellaris RNA FISH probe sets were used (Biosearch Technologies, Novato,
336 CA, USA) (Table S2) as previously described (80). Host-cell nuclei were counterstained
337 with DAPI during hybridization. Subsequently, the samples were refixed in 4% PFA for
338 7 h at 4°C as described (81) with minor modifications. Then, bacteriocytes were washed
339 thrice in PBSTx and blocked with 1% gelatin in PBS for 30 min at 25°C. After blocking,
340 bacteriocytes were incubated with the KDEL ER marker antibody (10C3) (Santa Cruz,
341 Dallas, TX, USA; cat. no. sc-58774) diluted (1:50) in PBS containing 1% gelatin and
342 0.05% Tween 20 overnight at 4°C. Bacteriocytes were washed thrice in PBSTx and then
343 incubated with Alexa Fluor Plus 555- or 647-conjugated goat anti-mouse IgG secondary
344 antibody (Thermo Fisher Scientific, Waltham, MA, USA) at a dilution of 1:100 for 3 h at
345 25°C.
346

Laser confocal microscopy. Samples were mounted with ProLong Diamond (Thermo Fisher Scientific). Images were obtained using a LSM5 Pascal or LSM710 microscope and analyzed using LSM5 Pascal Image and LSM ZEN2009 software (Carl Zeiss, Oberkochen, Germany).

Cytological staining. Staining bacteriocytes was performed as described previously (82), with some modifications. Bacteriocytes were dissected from female *B. tabaci* MED Q1 (Table S1) within 3 d after adult eclosion in Buffer A (35 mM Tris–HCl, pH 7.6, containing 10 mM $MgCl_2$, 25 mM KCl, and 250 mM sucrose) and stained with 4 μM SYTO16 (Thermo Fisher Scientific, Waltham, MA, USA) for nucleic acids (bacteria and host) and 4 μM ER-Tracker Red (Thermo Fisher Scientific) for ER in Buffer A for 2 h at 37°C on the SkyLight Glass Base Dish 3971-035-SK (IWAKI, Shizuoka, Japan). Images were obtained using a laser confocal microscope (LSM710) and analyzed using the LSM software ZEN2009 (Carl Zeiss, Oberkochen, Germany).

Statistics. To evaluate differences in the symbiont titers between females and males at each adult stage (days 1, 15 and 30), the Mann-Whitney U test with Bonferroni's correction was adopted. Analyses were conducted with R v.3.5.3 software (http://www.r-project.org).

Acknowledgements

We thank Y. Horita, D. Hwang, K. Moronaga, N. Murakami, Y. Utsuno, and M. Watanabe for technical assistance; N. Haruyama, K. Kijima, T. Kitamura, J. Ohnishi, I. Ohta, and T. Uesato for providing insect samples; and S. Egoshi, K. Dodo and M. Yoshida for useful comments. Part of this study was supported by JSPS KAKENHI Grant Number 18K05673 (to T.T.) and grants from the Project of the NARO Bio-oriented Technology Research Advancement Institution (Research program on the development of innovative technology). A.F. was supported by grants from the RIKEN Special Postdoctoral Researcher (SPDR) Program and Leading Initiative for Excellent Young Researchers (LEADER) Program.

References

1. Buchner P. 1965. Endosymbiosis of animals with plant microorganisms. 909 pp. John Wiley and Sons, New York, NY.
2. Moran NA, McCutcheon JP, Nakabachi A. 2008. Genomics and evolution of heritable bacterial symbionts. Annu Rev Genet 42:165-190.
3. Koga R, Bennett GM, Cryan JR, Moran NA. 2013. Evolutionary replacement of obligate symbionts in an ancient and diverse insect lineage. Environ Microbiol 15:2073-2081.
4. Noda H, Watanabe K, Kawai S, Yukuhiro F, Miyoshi T, Tomizawa M, Koizumi Y, Nikoh N, Fukatsu T. 2012. Bacteriome-associated endosymbionts of the green rice leafhopper Nephotettix cincticeps (Hemiptera: Cicadellidae). Appl Entomol

Zool 47:217-225.

5. Tsuchida T, Koga R, Horikawa M, Tsunoda T, Maoka T, Matsumoto S, Simon JC, Fukatsu T. 2010. Symbiotic bacterium modifies aphid body color. Science 330:1102-1104.

6. Matsuura Y, Koga R, Nikoh N, Meng XY, Hanada S, Fukatsu T. 2009. Huge symbiotic organs in giant scale insects of the genus *Drosicha* (Coccoidea: Monophlebidae) harbor flavobacterial and enterobacterial endosymbionts. Zoolog Sci 26:448-456.

7. Nakabachi A, Ueoka R, Oshima K, Teta R, Mangoni A, Gurgui M, Oldham NJ, van Echten-Deckert G, Okamura K, Yamamoto K, Inoue H, Ohkuma M, Hongoh Y, Miyagishima SY, Hattori M, Piel J, Fukatsu T. 2013. Defensive bacteriome symbiont with a drastically reduced genome. Curr Biol 23:1478-1484.

8. Manzano-Marin A, Szabo G, Simon JC, Horn M, Latorre A. 2017. Happens in the best of subfamilies: establishment and repeated replacements of co-obligate secondary endosymbionts within Lachninae aphids. Environ Microbiol 19:393-408.

9. Matsuura Y, Moriyama M, Lukasik P, Vanderpool D, Tanahashi M, Meng XY, McCutcheon JP, Fukatsu T. 2018. Recurrent symbiont recruitment from fungal parasites in cicadas. Proc Natl Acad Sci U S A 115:E5970-E5979.

10. Manzano-Marin A, Simon JC, Latorre A. 2016. Reinventing the Wheel and Making It Round Again: Evolutionary Convergence in *Buchnera-Serratia* Symbiotic Consortia between the Distantly Related Lachninae Aphids *Tuberolachnus salignus* and *Cinara cedri*. Genome Biol Evol 8:1440-1458.

11. Toenshoff ER, Penz T, Narzt T, Collingro A, Schmitz-Esser S, Pfeiffer S, Klepal

417 W, Wagner M, Weinmaier T, Rattei T, Horn M. 2012. Bacteriocyte-associated
418 gammaproteobacterial symbionts of the *Adelges nordmannianae*/*piceae* complex
419 (Hemiptera: Adelgidae). ISME J 6:384-396.
420 12. Monnin D, Jackson R, Kiers ET, Bunker M, Ellers J, Henry LM. 2020. Parallel
421 evolution in the integration of a co-obligate aphid symbiosis. Curr Biol 30:1949-
422 1957 e6.
423 13. Renoz F, Ambroise J, Bearzatto B, Fakhour S, Parisot N, Ribeiro Lopes M, Gala
424 JL, Calevro F, Hance T. 2022. The di-symbiotic systems in the aphids *Sipha*
425 *maydis* and *Periphyllus lyropictus* provide a contrasting picture of recent co-
426 obligate nutritional endosymbiosis in aphids. Microorganisms 10:1360.
427 14. Chomicki G, Werner GDA, West SA, Kiers ET. 2020. Compartmentalization drives
428 the evolution of symbiotic cooperation. Philos Trans R Soc Lond B Biol Sci
429 375:20190602.
430 15. Kanakala S, Ghanim M. 2019. Global genetic diversity and geographical
431 distribution of *Bemisia tabaci* and its bacterial endosymbionts. PLoS One
432 14:e0213946.
433 16. Gueguen G, Vavre F, Gnankine O, Peterschmitt M, Charif D, Chiel E, Gottlieb Y,
434 Ghanim M, Zchori-Fein E, Fleury F. 2010. Endosymbiont metacommunities,
435 mtDNA diversity and the evolution of the *Bemisia tabaci* (Hemiptera:
436 Aleyrodidae) species complex. Mol Ecol 19:4365-4376.
437 17. Tsagkarakou A, Mouton L, Kristoffersen JB, Dokianakis E, Grispou M, Bourtzis
438 K. 2012. Population genetic structure and secondary endosymbionts of Q *Bemisia*
439 *tabaci* (Hemiptera: Aleyrodidae) from Greece. Bull Entomol Res 102:353-365.
440 18. GnankinÉ O, Mouton L, Henri H, Terraz G, HoundetÉ T, Martin T, Vavre F,

Fleury F. 2013. Distribution of *Bemisia tabaci* (Homoptera: Aleyrodidae) biotypes and their associated symbiotic bacteria on host plants in West Africa. Insect Conservation and Diversity 6:411-421.

19. Bing XL, Ruan YM, Rao Q, Wang XW, Liu SS. 2013. Diversity of secondary endosymbionts among different putative species of the whitefly *Bemisia tabaci*. Insect Sci 20:194-206.

20. Fujiwara A, Maekawa K, Tsuchida T. 2015. Genetic groups and endosymbiotic microbiota of the *Bemisia tabaci* species complex in Japanese agricultural sites. J Appl Entomol 139:55–66.

21. Zchori-Fein E, Lahav T, Freilich S. 2014. Variations in the identity and complexity of endosymbiont combinations in whitefly hosts. Front Microbiol 5:310.

22. Marubayashi JM, Kliot A, Yuki VA, Rezende JA, Krause-Sakate R, Pavan MA, Ghanim M. 2014. Diversity and localization of bacterial endosymbionts from whitefly species collected in Brazil. PLoS One 9:e108363.

23. Karut K, Karaca MM, Döker I, Kazak C. 2017. Analysis of Species, Subgroups, and Endosymbionts of *Bemisia tabaci* (Hemiptera: Aleyrodidae) From Southwestern Cotton Fields in Turkey. Environ Entomol 46:1035-1040.

24. Su Q, Oliver KM, Pan H, Jiao X, Liu B, Xie W, Wang S, Wu Q, Xu B, White JA, Zhou X, Zhang Y. 2013. Facultative symbiont *Hamiltonella* confers benefits to *Bemisia tabaci* (Hemiptera: Aleyrodidae), an invasive agricultural pest worldwide. Environ Entomol 42:1265-71.

25. Su Q, Xie W, Wang S, Wu Q, Liu B, Fang Y, Xu B, Zhang Y. 2014. The endosymbiont *Hamiltonella* increases the growth rate of its host *Bemisia tabaci* during periods of nutritional stress. PLoS One 9: e89002.

26. Rao Q, Rollat-Farnier PA, Zhu DT, Santos-Garcia D, Silva FJ, Moya A, Latorre A, Klein CC, Vavre F, Sagot MF, Liu SS, Mouton L, Wang XW. 2015. Genome reduction and potential metabolic complementation of the dual endosymbionts in the whitefly *Bemisia tabaci*. BMC Genomics 16:226.

27. Chen W, Hasegawa DK, Kaur N, Kliot A, Pinheiro PV, Luan J, Stensmyr MC, Zheng Y, Liu W, Sun H, Xu Y, Luo Y, Kruse A, Yang X, Kontsedalov S, Lebedev G, Fisher TW, Nelson DR, Hunter WB, Brown JK, Jander G, Cilia M, Douglas AE, Ghanim M, Simmons AM, Wintermantel WM, Ling KS, Fei Z. 2016. The draft genome of whitefly *Bemisia tabaci* MEAM1, a global crop pest, provides novel insights into virus transmission, host adaptation, and insecticide resistance. BMC Biol 14:110.

28. Xie W, Yang X, Chen C, Yang Z, Guo L, Wang D, Huang J, Zhang H, Wen Y, Zhao J, Wu Q, Wang S, Coates BS, Zhou X, Zhang Y. 2018. The invasive MED/Q *Bemisia tabaci* genome: a tale of gene loss and gene gain. BMC Genomics 19:68.

29. Wang YB, Ren FR, Yao YL, Sun X, Walling LL, Li NN, Bai B, Bao XY, Xu XR, Luan JB. 2020. Intracellular symbionts drive sex ratio in the whitefly by facilitating fertilization and provisioning of B vitamins. ISME J 14:2923-2935.

30. Ankrah NYD, Luan J, Douglas AE. 2017. Cooperative Metabolism in a Three-Partner Insect-Bacterial Symbiosis Revealed by Metabolic Modeling. J Bacteriol 199.

31. Gottlieb Y, Ghanim M, Gueguen G, Kontsedalov S, Vavre F, Fleury F, Zchori-Fein E. 2008. Inherited intracellular ecosystem: symbiotic bacteria share bacteriocytes in whiteflies. FASEB J 22:2591-2599.

32. Skaljac M, Zanic K, Ban SG, Kontsedalov S, Ghanim M. 2010. Co-infection and

localization of secondary symbionts in two whitefly species. BMC Microbiology 10:142.

33. Li NN, Jiang S, Lu KY, Hong JS, Wang YB, Yan JY, Luan JB. 2022. Bacteriocyte development is sexually differentiated in *Bemisia tabaci*. Cell Rep 38:110455.

34. Su Q, Xie W, Wang S, Wu Q, Ghanim M, Zhang Y. 2014. Location of symbionts in the whitefly *Bemisia tabaci* affects their densities during host development and environmental stress. PLoS One 9:e91802.

35. Koga R, Tsuchida T, Fukatsu T. 2003. Changing partners in an obligate symbiosis: a facultative endosymbiont can compensate for loss of the essential endosymbiont Buchnera in an aphid. Proc Biol Sci 270:2543-2550.

36. Sakurai M, Koga R, Tsuchida T, Meng XY, Fukatsu T. 2005. *Rickettsia* symbiont in the pea aphid *Acyrthosiphon pisum*: novel cellular tropism, effect on host fitness, and interaction with the essential symbiont Buchnera. Appl Environ Microbiol 71:4069-4075.

37. Simonet P, Duport G, Gaget K, Weiss-Gayet M, Colella S, Febvay G, Charles H, Vinuelas J, Heddi A, Calevro F. 2016. Direct flow cytometry measurements reveal a fine-tuning of symbiotic cell dynamics according to the host developmental needs in aphid symbiosis. Sci Rep 6:19967.

38. Vigneron A, Masson F, Vallier A, Balmand S, Rey M, Vincent-Monegat C, Aksoy E, Aubailly-Giraud E, Zaidman-Remy A, Heddi A. 2014. Insects recycle endosymbionts when the benefit is over. Curr Biol 24:2267-2273.

39. Luan JB, Shan HW, Isermann P, Huang JH, Lammerding J, Liu SS, Douglas AE. Cellular and molecular remodelling of a host cell for vertical transmission of bacterial symbionts. Proc R Soc B 283:20160580.

513 40. Ren FR, Sun X, Wang TY, Yao YL, Huang YZ, Zhang X, Luan JB. Biotin
514 provisioning by horizontally transferred genes from bacteria confers animal fitness
515 benefits. ISME J 14:2542-2553.
516 41. Gottlieb Y, Ghanim M, Chiel E, Gerling D, Portnoy V, Steinberg S, Tzuri G,
517 Horowitz AR, Belausov E, Mozes-Daube N, Kontsedalov S, Gershon M, Gal S,
518 Katzir N, Zchori-Fein E. 2006. Identification and localization of a *Rickettsia* sp. in
519 *Bemisia tabaci* (Homoptera: Aleyrodidae). Appl Environ Microbiol 72:3646-3652.
520 42. Himler AG, Adachi-Hagimori T, Bergen JE, Kozuch A, Kelly SE, Tabashnik BE,
521 Chiel E, Duckworth VE, Dennehy TJ, Zchori-Fein E, Hunter MS. 2011. Rapid
522 spread of a bacterial symbiont in an invasive whitefly is driven by fitness benefits
523 and female bias. Science 332:254-256.
524 43. Costa HS, Toscano NC, Henneberry TJ. 1996. Mycetocyte inclusion in the oocytes
525 of *Bemisia argentifolii* (Homoptera: Aleyrodidae). Ann Entomol Soc Am 89:694–
526 699.
527 44. Luan J, Sun X, Fei Z, Douglas AE. 2018. Maternal inheritance of a single somatic
528 animal cell displayed by the bacteriocyte in the whitefly *Bemisia tabaci*. Curr Biol
529 28:459-465 e3.
530 45. Tang XT, Cai L, Shen Y, Du YZ. 2018. Diversity and evolution of the
531 endosymbionts of *Bemisia tabaci* in China. PeerJ 6:e5516.
532 46. Mound LA, Halsey SH. 1978. Whitefly of the world : a systematic catalogue of
533 the Aleyrodidae (Homoptera) with host plant and natural enemy data. 340 pp. John
534 Wiley and Sons, Chichester, UK.
535 47. Kapantaidaki DE, Ovčarenko I, Fytrou N, Knott KE, Bourtzis K, Tsagkarakou A.
536 2015. Low levels of mitochondrial DNA and symbiont diversity in the worldwide

agricultural pest, the greenhouse whitefly *Trialeurodes vaporariorum* (Hemiptera: Aleyrodidae). J Hered 106:80-92.

48. Skaljac M, Zanic K, Hrncic S, Radonjic S, Perovic T, Ghanim M. 2013. Diversity and localization of bacterial symbionts in three whitefly species (Hemiptera: Aleyrodidae) from the east coast of the Adriatic Sea. Bull Entomol Res 103:48-59.

49. Santos-Garcia D, Juravel K, Freilich S, Zchori-Fein E, Latorre A, Moya A, Morin S, Silva FJ. 2018. To B or Not to B: Comparative Genomics Suggests *Arsenophonus* as a Source of B Vitamins in Whiteflies. Front Microbiol 9:2254.

50. Hardin G. 1960. The competitive exclusion principle. Science 131:1292-1297.

51. Chesson P. 2000. Mechanisms of maintenance of species diversity. Annu. Rev. Ecol. Syst 31:343-366.

52. Levine JM, HilleRisLambers J. 2009. The importance of niches for the maintenance of species diversity. Nature 461:254-257.

53. Xu XR, Li NN, Bao XY, Douglas AE, Luan JB. 2020. Patterns of host cell inheritance in the bacterial symbiosis of whiteflies. Insect Sci 27:938-946.

54. McCutcheon JP, Moran NA. 2007. Parallel genomic evolution and metabolic interdependence in an ancient symbiosis. Proc Natl Acad Sci U S A 104:19392-19397.

55. McCutcheon JP, Moran NA. 2010. Functional convergence in reduced genomes of bacterial symbionts spanning 200 My of evolution. Genome Biol Evol 2:708-718.

56. McCutcheon JP, McDonald BR, Moran NA. 2009. Convergent evolution of metabolic roles in bacterial co-symbionts of insects. Proc Natl Acad Sci U S A 106:15394-15399.

561 57. Koga R, Moran NA. 2014. Swapping symbionts in spittlebugs: evolutionary
562 replacement of a reduced genome symbiont. ISME J 8:1237-1246.
563 58. Szabo G, Schulz F, Manzano-Marin A, Toenshoff ER, Horn M. 2022.
564 Evolutionarily recent dual obligatory symbiosis among adelgids indicates a
565 transition between fungus- and insect-associated lifestyles. ISME J 16:247-256.
566 59. Meseguer AS, Manzano-Marín A, Coeur d'Acier A, Clamens AL, Godefroid M,
567 Jousselin E. 2017. *Buchnera* has changed flatmate but the repeated replacement of
568 co-obligate symbionts is not associated with the ecological expansions of their
569 aphid hosts. Mol Ecol 26:2363–2378.
570 60. Weglarz KM, Havill NP, Burke GR, von Dohlen CD. 2018. Partnering With a
571 Pest: Genomes of Hemlock Woolly Adelgid Symbionts Reveal Atypical
572 Nutritional Provisioning Patterns in Dual-Obligate Bacteria. Genome Biol Evol
573 10:1607-1621.
574 61. Luan JB, Chen W, Hasegawa DK, Simmons AM, Wintermantel WM, Ling KS,
575 Fei Z, Liu SS, Douglas AE. 2015. Metabolic Coevolution in the Bacterial
576 Symbiosis of Whiteflies and Related Plant Sap-Feeding Insects. Genome Biol
577 Evol 7:2635-2647.
578 62. von Dohlen CD, Kohler S, Alsop ST, McManus WR. 2001. Mealybug beta-
579 proteobacterial endosymbionts contain gamma-proteobacterial symbionts. *Nature*
580 412:433–436.
581 63. Husnik F, Nikoh N, Koga R, Ross L, Duncan RP, Fujie M, Tanaka M, Satoh N,
582 Bachtrog D, Wilson AC, von Dohlen CD, Fukatsu T, McCutcheon JP. 2013.
583 Horizontal gene transfer from diverse bacteria to an insect genome enables a
584 tripartite nested mealybug symbiosis. Cell 153:1567-1578.

64. Husnik F, McCutcheon JP. 2016. Repeated replacement of an intrabacterial symbiont in the tripartite nested mealybug symbiosis. Proc Natl Acad Sci U S A 113:E5416- E5424.

65. Szabó G, Schulz F, Toenshoff ER, Volland JM, Finkel OM, Belkin S, Horn M. 2017. Convergent patterns in the evolution of mealybug symbioses involving different intrabacterial symbionts. ISME J 11:715-726.

66. Santos-Garcia D, Vargas-Chavez C, Moya A, Latorre A, Silva FJ. 2015. Genome evolution in the primary endosymbiont of whiteflies sheds light on their divergence. Genome Biol Evol 7:873-888.

67. Mouton L, Henri H, Romba R, Belgaidi Z, Gnankiné O, Vavre F. 2022. Analyses of symbiotic bacterial communities in the plant pest *Bemisia tabaci* reveal high prevalence of *Candidatus* Hemipteriphilus asiaticus on the African continent. Peer Community J 2:e20.

68. Arasaki K, Toomre DK, Roy CR. 2012. The *Legionella pneumophila* effector DrrA is sufficient to stimulate SNARE-dependent membrane fusion. Cell Host Microbe 11:46-57.

69. Starr T, Child R, Wehrly TD, Hansen B, Hwang S, Lopez-Otin C, Virgin HW, Celli J. 2012. Selective subversion of autophagy complexes facilitates completion of the *Brucella* intracellular cycle. Cell Host Microbe 11:33-45.

70. Mehlitz A, Karunakaran K, Herweg JA, Krohne G, van de Linde S, Rieck E, Sauer M, Rudel T. 2014. The chlamydial organism Simkania negevensis forms ER vacuole contact sites and inhibits ER-stress. Cell Microbiol doi:10.1111/cmi.12278.

71. Escoll P, Mondino S, Rolando M, Buchrieser C. 2016. Targeting of host organelles

by pathogenic bacteria: a sophisticated subversion strategy. Nat Rev Microbiol 14:5-19.

72. Newton IL, Savytskyy O, Sheehan KB. 2015. Wolbachia utilize host actin for efficient maternal transmission in Drosophila melanogaster. PLoS Pathog 11:e1004798.

73. Sheehan KB, Martin M, Lesser CF, Isberg RR, Newton IL. 2016. Identification and Characterization of a Candidate *Wolbachia pipientis* Type IV Effector That Interacts with the Actin Cytoskeleton. mBio 7.

74. Simonet P, Gaget K, Balmand S, Ribeiro Lopes M, Parisot N, Buhler K, Duport G, Vulsteke V, Febvay G, Heddi A, Charles H, Callaerts P, Calevro F. 2018. Bacteriocyte cell death in the pea aphid/*Buchnera* symbiotic system. Proc Natl Acad Sci U S A 115:E1819-E1828.

75. Fattouh N, Cazevieille C, Landmann F. 2019. *Wolbachia* endosymbionts subvert the endoplasmic reticulum to acquire host membranes without triggering ER stress. PLoS Negl Trop Dis 13:e0007218.

76. Strunov A, Schmidt K, Kapun M, Miller WJ. 2022. Restriction of *Wolbachia* Bacteria in Early Embryogenesis of Neotropical *Drosophila* Species via Endoplasmic Reticulum-Mediated Autophagy. mBio 13:e0386321.

77. Fukatsu T. 1999. Acetone preservation: a practical technique for molecular analysis. Mol. Ecol. 8:1935–1945.

78. Tsuchida T, Koga R, Fujiwara A, Fukatsu T. 2014. Phenotypic Effect of "*Candidatus* Rickettsiella viridis," a Facultative Symbiont of the Pea Aphid (*Acyrthosiphon pisum*), and Its Interaction with a Coexisting Symbiont. Appl Environ Microbiol 80:525-533.

633 79. Koga R, Tsuchida T, Fukatsu T. 2009. Quenching autofluorescence of insect
634 tissues for in situ detection of endosymbionts. Appl Entomol Zool 44:281-291.
635 80. De Clerck C, Fujiwara A, Joncour P, Leonard S, Felix ML, Francis F, Jijakli MH,
636 Tsuchida T, Massart S. 2015. A metagenomic approach from aphid's hemolymph
637 sheds light on the potential roles of co-existing endosymbionts. Microbiome 3:63.
638 81. Larsen P, Nielsen JL, Otzen D, Nielsen PH. 2008. Amyloid-like adhesins
639 produced by floc-forming and filamentous bacteria in activated sludge. Appl
640 Environ Microbiol 74:1517-1526.
641 82. Nishikori K, Morioka K, Kubo T, Morioka M. 2009. Age- and morph-dependent
642 activation of the lysosomal system and *Buchnera* degradation in aphid
643 endosymbiosis. J Insect Physiol 55:351-357.

644

645

646

647 **Figure Legends**

648 Figure 1. Localization of *Portiera* (red) and *Hamiltonella* (green) in bacteriocytes of
649 *Bemisia tabaci*. (*A*–*C*) MEAM1: (*A*) bacteriocytes dissected from an adult female, (*B*) A
650 3-day-old egg, and (*C*) a bacteriocyte dissected from a fourth-instar nymph. (*D*–*F*) MED
651 Q1 strain: (*D*) Bacteriocytes of the fourth-instar nymph, (*E*) enlarged image of the regions
652 indicated by a yellow square in (*D*), and (*F*) a bacteriocyte just before entering the egg in
653 a teneral adult female. In (*A*–*C*, *E*, and *F*), orthogonal views of Z-stack images are shown;
654 red and blue dashed lines indicate corresponding points in the orthogonal planes. In (*B*, *D*,
655 *E,* and *F*), host nuclear DNA is visualized in blue. In (*F*), white dashed lines indicate the

656 outline of the egg. Bars, 20 μm.

657

658 Figure 2. Transmission electron micrographs (TEM) of a bacteriocyte in *B. tabaci*
659 MEAM1. (*A*) Unstructured hypertrophic bacteria (*Portiera*) in the cytoplasm and rod-
660 shaped bacteria (*Hamiltonella*) around the nucleus of the bacteriocyte. (*B*) Enlarged image
661 of *Hamiltonella*. N, nucleus of a bacteriocyte; P, *Portiera*; H, *Hamiltonella*. Blue
662 arrowhead, ER-like structures surrounding *Hamiltonella*. Bars, 2 μm.

663

664 Figure 3. Localization of *Hamiltonella* and the ER in a bacteriocyte of a young adult
665 female (1–5 d after eclosion) of MEAM1(*A*) and MED Q1(*B*). Orthogonal views of Z-
666 stack images are shown. Red and blue dashed lines indicate corresponding points in the
667 orthogonal planes. *Hamiltonella* and ER are shown in green and violet, respectively.
668 Panels in the bottom right corner of each figure are DAPI-stained images, showing nuclei
669 in the center of the bacteriocytes and *Portiera* and *Hamiltonella* around the nuclei. Yellow
670 dashed lines indicate the outline of the bacteriocytes. Bars, 20 μm.

671

672 Figure 4. Localization of *Portiera* (red) and *Arsenophonus* (green) in a putative young
673 adult female *B. tabaci* Asia II 6. (*A*) Bacteriocytes in the abdomen. (*B*) developing egg
674 within the female. Orthogonal views of Z-stack images are shown. Red and blue dashed
675 lines indicate corresponding points in the orthogonal planes. Host nuclear DNA is
676 visualized in blue. In (*B*), yellow dashed lines indicate the outline of the egg. Bars, 50 μm.

677

678 Figure 5. Localization of *Portiera* (red), *Arsenophonus* (green), and the ER (violet) in
679 bacteriocytes of *Trialeurodes vaporariorum*. (*A*) FISH image and (*B*)

680 immunohistochemistry combined with FISH (*B*). Orthogonal views of Z-stack images are
681 shown. Red and blue dashed lines indicate corresponding points in the orthogonal planes.
682 In (*B*), panel in the bottom right corner is DAPI-stained images and yellow dashed lines
683 indicate the outline of a bacteriocyte. Bars, 20 μm.
684
685 Figure 6. Phylogenetic relationships among whiteflies and their symbiotic system in
686 bacteriocytes. Numbers at internal nodes indicate the divergence date (Mya: million years
687 ago) estimated by Santos-Garcia *et al.* (66). The size of bacteriocytes is shown on the
688 same scale.
689
690
691 **Supplemental Movie Legend**
692 Movie S1. Z-stack images of bacteriocytes harboring *Portiera* (red) and *Hamiltonella*
693 (green) in *B. tabaci* MEAM1. Bar, 50 μm. In total, 55 spatially consecutive images were
694 collected by confocal microscopy (depth interval = 0.5 μm) and were processed using
695 Zeiss LSM5 Pascal Image software. Nuclei in the center of bacteriocytes are not shown
696 in the movie to clarify the localization patterns of the two symbionts.
697
698
699 **Supplemental Figure Legends**
700 Fig. S1. Population dynamics of symbionts in *B. tabaci* MEAM1. Bacterial titers of
701 *Portiera* (*A*) and *Hamiltonella* (*B*) were measured by quantitative PCR in terms of 16S
702 ribosomal RNA gene copies per insect. Each dot represents an individual; filled diamonds,

703 eggs and nymphs; open circles, adult females; gray triangles, adult males; n = 2 for eggs,
704 n = 10 for others. Asterisks indicate statistically significant differences ($P < 0.001$),
705 whereas "ns" indicates not significant ($P > 0.05$). Note that symbiont titer in an egg was
706 calculated by averaging acquired value of 10 individuals.
707
708 Fig. S2. *In vivo* localization of facultative symbionts around bacteriocytes in a young adult
709 *B. tabaci*. Female (*A*) and male (*B*) within day 5 after eclosion in MEAM1. Female (*C*)
710 and male (*D*) at day 1 after eclosion in MED Q1. Green indicates *Rickettsia* (*A* and *B*) or
711 *Cardinium* (*C* and *D*). *Portiera* is shown in red. Host nuclear DNA is visualized in blue.
712 Bars, 50 μm.
713
714 Fig. S3. *In vivo* localization of *Portiera* (red) and *Hamiltonella* (green) in bacteriocytes of
715 *B. tabaci* MEAM1. (*A*) Adult female at day 1 after eclosion, (*B*) adult male at day 1 after
716 eclosion, (*C*) adult female at day 15 after eclosion, and (*D*) adult male at day 15 after
717 eclosion. N, bacteriocyte nucleus; Bars, 50 μm.
718
719 Fig S4. Detection of symbionts and the ER by FISH and immunohistochemistry. The
720 bacteriocyte in a *B tabaci* MEAM1 young adult female at day 1 to 5 after eclosion (*A*),
721 old female at day 15 after eclosion (*B*), old male at day 15 after eclosion (*C*), MED Q1
722 young adult female at day 1 to 5 after eclosion (*D*), putative young female of *B. tabaci*
723 Asia II 6 (*E*), and *T. vaporariorum* young adult female at day 1 to 5 after eclosion (*F*).
724 The images in *A, D,* and *F* correspond to Fig. 3*A* and *B*, and 5*B*, respectively. Panels for
725 DNA (*first column*), symbiont (*Hamiltonella* or *Arsenophonus*) (*second column*), ER
726 (*third column*), and merged image of the ER and symbiont (*fourth column*) are shown. In

(*B*, *C,* and *F*), panels for *Portiera* are added in the fifth column. DAPI-stained images in the first column show nuclei in the center of bacteriocytes, and *Portiera* and *Hamiltonella* around the nuclei. In merged panels, the ER is shown in violet and *Hamiltonella* or *Arsenophonus* is shown in green. Yellow dashed lines indicate outlines of the bacteriocytes. Bars, 20 μm. Relatively weak signals of *Arsenophonus* and the ER in (*E*) can likely be explained by the use of acetone-preserved samples.

Fig. S5. *In vivo* localization of the ER and endosymbionts in living bacteriocytes of *B. tabaci* MED Q1. Orthogonal view of Z-stack images is shown. Red and blue dashed lines indicate corresponding points in the orthogonal planes. DNA and ER are shown in green and violet, respectively. In the cytoplasm, *Portiera* and *Hamiltonella* were detected as unstructured hypertrophic bacteria (weak green) and rod-shaped bacteria (strong green), respectively. N, nucleus of the bacteriocyte; P, *Portiera*; H, *Hamiltonella*. Bar, 20 μm.

Fig. S6. Interdependent biosynthetic pathways of the essential amino acids in the co-obligate symbionts in whiteflies inferred from the published genomes. Lysine biosynthesis pathways in *(A) B. tabaci* MEAM1 (W. Chen*, et al.* BMC Biol. 14: 110, 2016) and MED Q1 (W. Xie*, et al.* BMC Genomics 19: 68, 2018). Genes of *Portiera*, *Hamiltonella,* and the host (candidate horizontally transferred genes) are indicated by magenta, green, and blue arrows, respectively. *(B)* Phenylalanine and tryptophan biosynthesis pathways in *T. vaporariorum* (D. Santos-Garcia, C. Vargas-Chavez, A. Moya, A. Latorre, F.J. Silva, Genome Biol. Evol. 7: 873–888, 2015; D. Santos-Garcia*,* K. Juravel, S. Freilich, E. Zchori-Fein, A. Latorre, A. Moya, S. Morin, F.J. Silva, Front. Microbiol. 9: 2254, 2018). Genes of *Portiera*, *Arsenophonus* and the host are indicated by magenta, green, and blue

751 arrows, respectively. Missing genes are indicated by dashed arrows. (*C*) Schematic of ER-
752 mediated habitat segregation and putative nutrient flow in the co-obligate symbiotic
753 system in whiteflies.
754
755 Fig. S7. Stages of *B. tabaci* MEAM1 development. Yellow cells in the egg or body are
756 bacteriocytes. Numbers of days on the arrow indicate the approximate durations under
757 laboratory conditions. Reproduction is frequently observed in young adults but rarely in
758 senescent adults. Bars, 0.1 mm.
759
760

Fig. 1

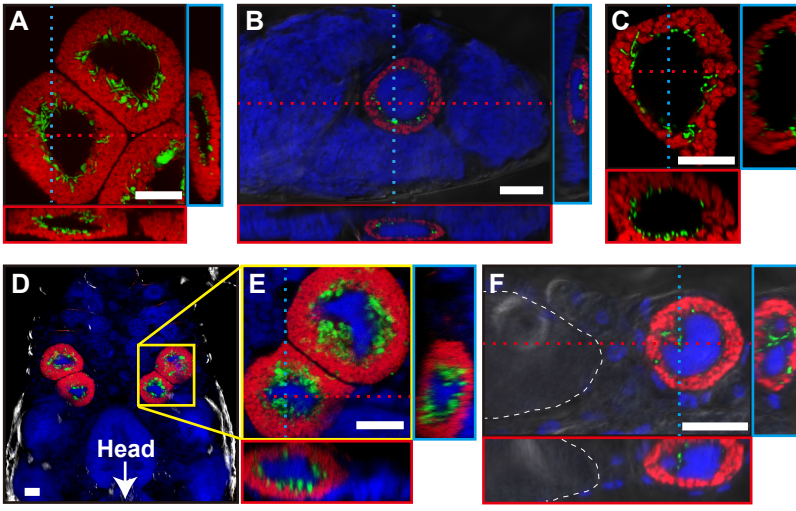

Figure 1. Localization of *Portiera* (red) and *Hamiltonella* (green) in bacteriocytes of *Bemisia tabaci*. (*A*–*C*) MEAM1: (*A*) bacteriocytes dissected from an adult female, (*B*) A 3-day-old egg, and (*C*) a bacteriocyte dissected from a fourth-instar nymph. (*D*–*F*) MED Q1 strain: (*D*) Bacteriocytes of the fourth-instar nymph, (*E*) enlarged image of the regions indicated by a yellow square in (*D*), and (*F*) a bacteriocyte just before entering the egg in a teneral adult female. In (*A*–*C*, *E*, and *F*), orthogonal views of *Z*-stack images are shown; red and blue dashed lines indicate corresponding points in the orthogonal planes. In (*B*, *D*, *E*, and *F*), host nuclear DNA is visualized in blue. In (*F*), white dashed lines indicate the outline of the egg. Bars, 20 μm.

Fig. 2

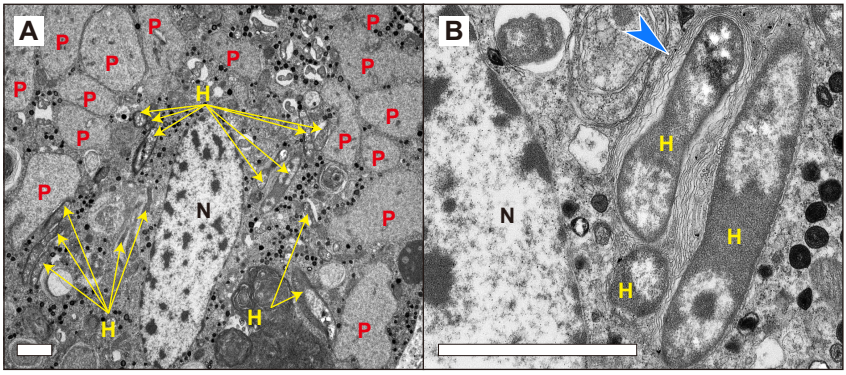

Figure 2. Transmission electron micrographs (TEM) of a bacteriocyte in *B. tabaci* MEAM1. (*A*) Unstructured hypertrophic bacteria (*Portiera*) in the cytoplasm and rod-shaped bacteria (*Hamiltonella*) around the nucleus of the bacteriocyte. (*B*) Enlarged image of *Hamiltonella*. N, nucleus of a bacteriocyte; P, *Portiera*; H, *Hamiltonella*. Blue arrowhead, ER-like structures surrounding *Hamiltonella*. Bars, 2 μm.

Fig. 3

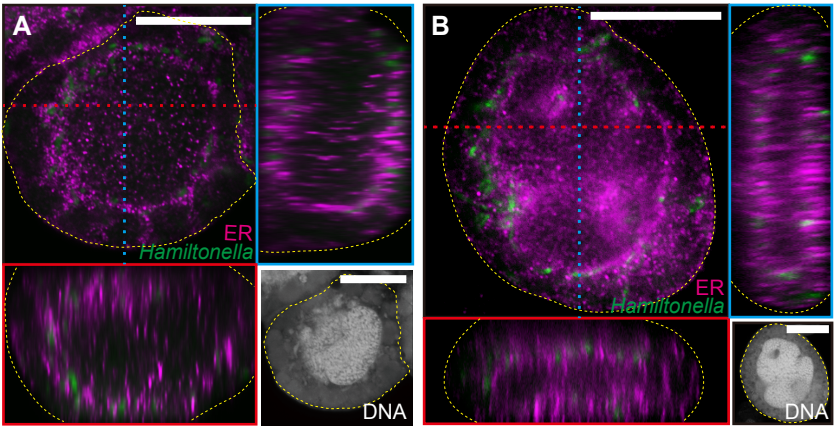

Figure 3. Localization of *Hamiltonella* and the ER in a bacteriocyte of a young adult female (1–5 d after eclosion) of MEAM1(*A*) and MED Q1(*B*). Orthogonal views of Z-stack images are shown. Red and blue dashed lines indicate corresponding points in the orthogonal planes. *Hamiltonella* and ER are shown in green and violet, respectively. Panels in the bottom right corner of each figure are DAPI-stained images, showing nuclei in the center of the bacteriocytes and *Portiera* and *Hamiltonella* around the nuclei. Yellow dashed lines indicate the outline of the bacteriocytes. Bars, 20 μm.

Fig. 4

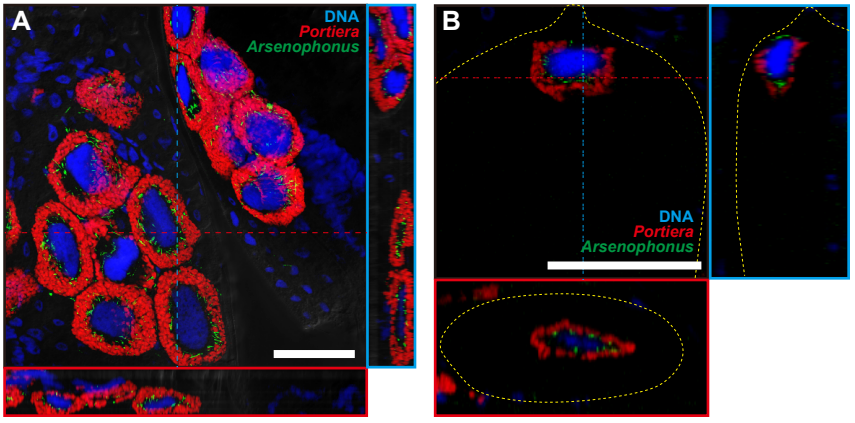

Figure 4. Localization of *Portiera* (red) and *Arsenophonus* (green) in a putative young adult female *B. tabaci* Asia II 6. (*A*) Bacteriocytes in the abdomen. (*B*) developing egg within the female. Orthogonal views of Z-stack images are shown. Red and blue dashed lines indicate corresponding points in the orthogonal planes. Host nuclear DNA is visualized in blue. In (*B*), yellow dashed lines indicate the outline of the egg. Bars, 50 μm.

Fig. 5

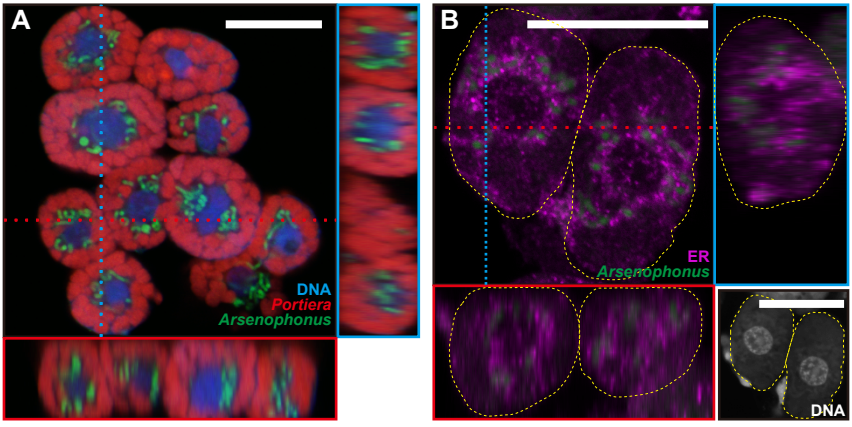

Figure 5. Localization of *Portiera* (red), *Arsenophonus* (green), and the ER (violet) in bacteriocytes of *Trialeurodes vaporariorum*. (*A*) FISH image and (*B*) immunohistochemistry combined with FISH (*B*). Orthogonal views of Z-stack images are shown. Red and blue dashed lines indicate corresponding points in the orthogonal planes. In (*B*), panel in the bottom right corner is DAPI-stained images and yellow dashed lines indicate the outline of a bacteriocyte. Bars, 20 μm.

Fig. 6

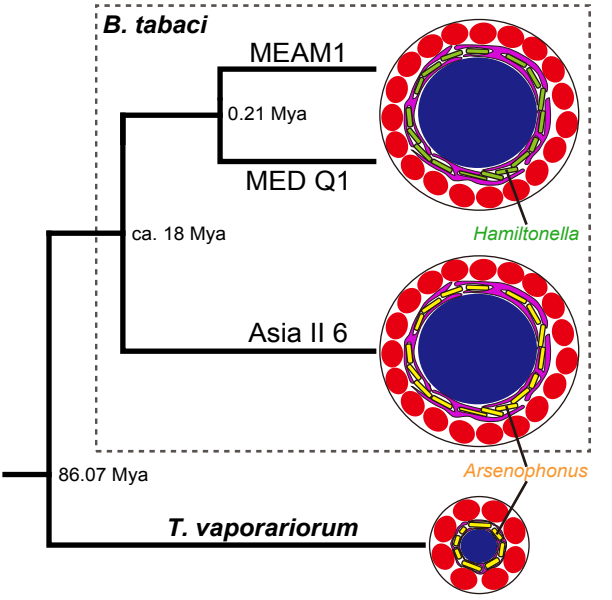

Figure 6. Phylogenetic relationships among whiteflies and their symbiotic system in bacteriocytes. Numbers at internal nodes indicate the divergence date (Mya: million years ago) estimated by Santos-Garcia *et al*. (64). The size of bacteriocytes is shown on the same scale.